International Journal of Current Engineering and Technology
ISSN 2277 - 4106

Available at http://inpressco.com/category/ijcet

Research Article

# A Comparative Study of Pure and Rare Earth Transition Metal Doped Bismuth Ferrite

Soumya Mukherjee[a*], Subhabrata Chakraborty[b], Siddhartha Mukherjee[a]

[a]Metallurgical and Material Engineering Department, Jadavpur University, Kolkata-700032, India
[b]School of Materials Science and Nanotechnology, Jadavpur University, Kolkata-700032, India

Accepted 25 Nov.2012, Available online 1Dec. 2012, **Vol.2, No.4(Dec. 2012)**

***Abstract***

*Pure and Rare Earth transition metal (7.5% and 10% lanthanum, yttrium) doped bismuth ferrite samples were synthesized through chemical solution route. Crystallization temperature around 450°C was observed from thermal analysis by DTA-TGA and subsequent XRD analysis of the annealed samples showed that the crystallites were mainly rhombohedral with R3c space group with an expected impurity phase. Morphological analysis using FESEM and AFM revealed the samples to be of agglomerated nature and optical analysis by UV-VIS spectroscopy showed a decrease and increase in the band gap due to La and Y doping respectively.*

***Keywords****: La/Y doped BFO, DTA-TGA, XRD, FESEM, AFM, UV-VIS etc.*

## 1. Introduction

Magnetoelectric coupling was first predicted in the 1960s, though it was first reportedly observed in naturally occurring multiferroic material chromium (III) oxide. However, the term 'Multiferroic' was first coined by Schimd in the year 1994 (G. Catalan *et al*, 1999). Bismuth ferrite is a room temperature single phase multiferroic material with distorted perovskite structure. It exhibits both ferroelectricity and antiferromagnetism (G type ordering) with the respective Curie and Néel temperatures at 1100K and 643K. The stereochemically active $6s^2$ lone pair of A-site cation $Bi^{3+}$ causes hybridization between empty 6p orbital of bismuth and 2p orbital of oxygen. This drives the off-centering of the cation towards the neighbouring anion, thus imparting ferroelectricity. In BFO, the spins are ferromagnetically coupled in pseudocubic (111) plane and antiferromagnetically in adjacent planes. Due to the canting of the antiferromagnetic sublattice, the material has weak ferromagnetism. However, spin cycloid being superimposed on it, the antiferromagnetic axis rotates through the crystal with a wavelength of about 62nm and thus the weak ferromagnetism get nullified (Y. Yao *et al*, 2011). The recent interest in this field is basically due to an observation that BFO films have a remanent polarization of about 15 times than that of bulk samples (G. Catalan *et al*, 1999).

It has been seen that BFO crystallites on doping with La or Y have shown structural distortions as well as improved ferroelectric properties. However the structural distortions are dependent upon the method of synthesis. Pulsed laser deposition on $Pt/TiO_2/SiO_2/Si$ has given monoclinic, orthorhombic and tetragonal structures (F. Gao *et al*, 2006; S. R. Das *et al*, 2006; F. Yan *et al*, 2010) whereas hydrothermal route does not change the structures of the doped samples (M. Hojamberdiev *et al*, 2009; Z. Chen *et al*, 2011; A. Chaudhuri *et al*, 2012; X. Yan *et al*, 2010; Y. Du *et al*, 2010). The band gap of BFO has also decreased due to doping (M. B. Bellakki *et al*, 2010). Thus rare earth doped BFO samples have shown much promise in the commercial field in context to fabrication of memory elements, sensors etc.

The aim of present investigation is to compare the morphological and structural changes in BFO due to doping with 7.5% and 10% lanthanum and yttrium along with the changes in the band gap of the material. These materials may have potential applications for photo catalytic behaviour in visible range.

## Experimental procedure

Stoichometric amounts of bismuth (III) nitrate pentahydrate (Merck, India) and iron (III) (Merck, India) nitrate nonahydrate were taken in a beaker with molar ratio of 1:1. Citric acid (Merck, India) was added to the beaker ensuring that the number of moles of citric acid be equal to the total number of moles of the combined nitrate salts of bismuth and iron. Then a few drops of distilled water were added in the beaker and the mixture was stirred in a magnetic stirrer for about 15 minutes. Finally, ethylene glycol was added to it such that the volumetric ratio of ethylene glycol (Merck, India) to citric acid

* Corresponding author: Tel.: +91-9830179414

maintained was 60:40 and the mixture was again stirred for 1 hour. The resulting solution was then heat treated in a pot furnace at 317°C to form an amorphous structure and finally at 450°C to crystallize the sample. To prepare 7.5% and 10% La and Y doped BFO crystallites, lanthanum (III) nitrate solution (Merck, India) and yttrium (III) nitrate hexahydrate salt (Merck, India) were added ensuring that the number of moles of nitrate salt of iron and that of nitrate salt/solution of bismuth along with La/Y be equal. After synthesis, the prepared samples were ground in an agate mortar and a part of it was dispersed in ethanol. The dispersed solution was then spin coated on glass slides for AFM studies. The thermal characterization for ascertaining the crystallization temperature was done by DTA-TGA (Perkin Elmer, Pyris Diamond 480). Rigaku ultima III XRD (Rigaku Ultima III) having source wavelength of Cu Kα = 1.54Å was used for phase identification of the samples along with crystallite size determination using Scherrer formula. Morphological analyses of the as prepared samples were done by FESEM (Hitachi, S-4800) and AFM (NT-MDT, Solver Model No.50BM-4). The band gap of the formed samples was determined by UV-VIS spectrometer (Perkin Elmer, Lambda 35).

**Results and discussions**

*DTA-TGA analyses*

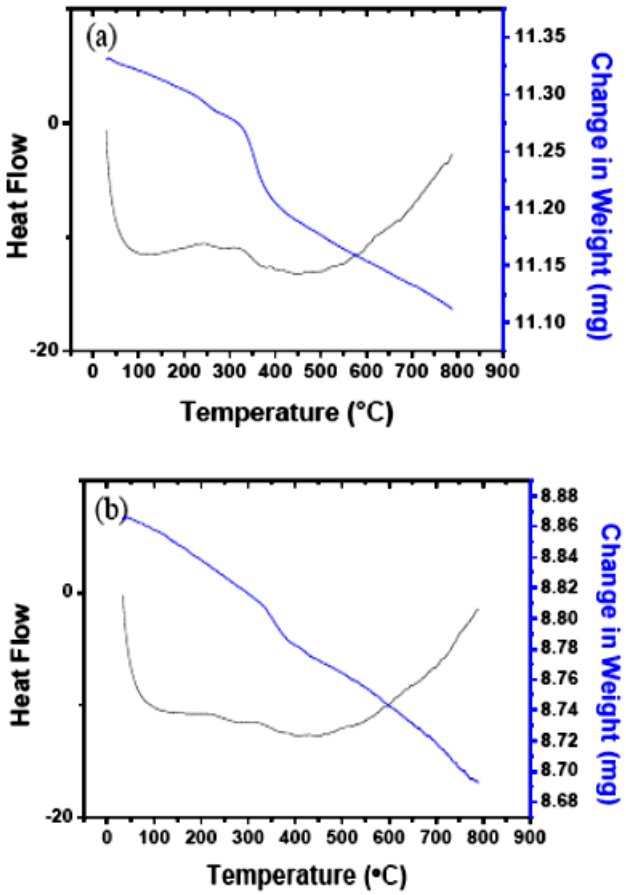


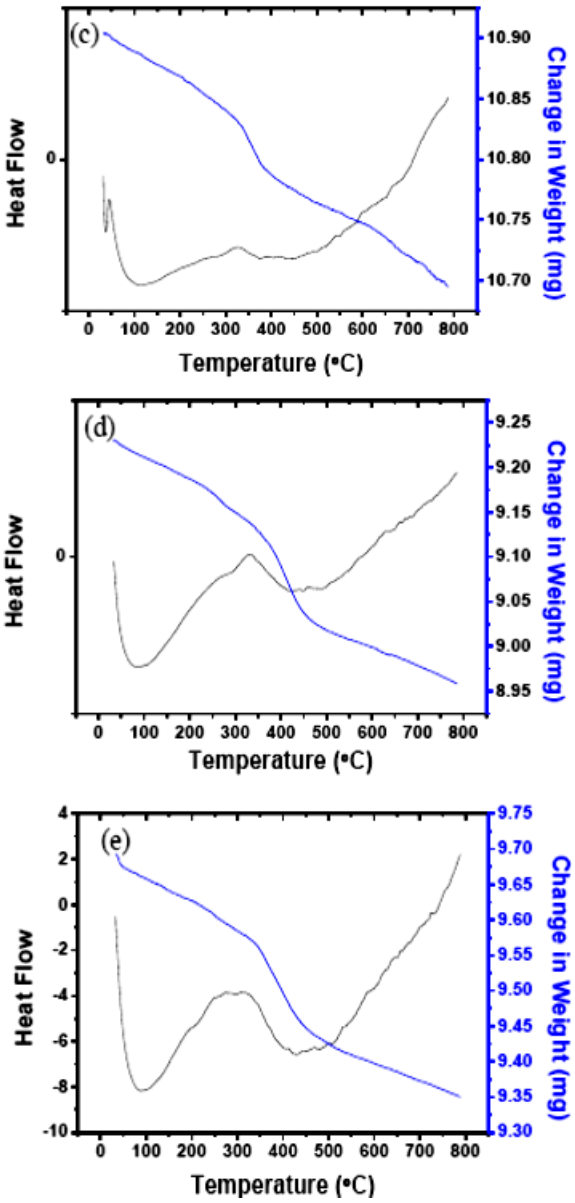


Figure 1: DTA-TGA curves of a) pure BFO; b) 7.5% La doped BFO; c) 10% La doped BFO; d) 7.5% Y doped BFO; e) 10% Y doped BFO

Figure 1 shows the DTA-TGA curves for the prepared samples. In all the curves endothermic peaks can be found around 100°C and minor peaks at 450°C. These peaks correspond to the dehydration and crystallization temperatures of all the samples. Thus, we determined that the crystallization temperature for proper phase development of the samples to be around 450°C. In the pure sample, an endothermic peak can be found at 330°C which can be attributed to the Néel temperature of BFO (643K). In case of doped samples, this peak shifts slightly towards the left. It was seen that with the increase in doping percentage, the peak shifts further towards right however, it remained on the left side compared to pure sample. In 7.5% La doped sample this peak was around 313°C and that for 10% La doped sample it was around 325°C. In case of Y doped samples this shift was less

pronounced. For 7.5% Y doped sample this peak can be found at around 327°C and the same peak for 10% Y doped sample was around 329°C. The corresponding weight change for 7.5% and 10% La doped samples was less in comparison to pure sample while that for both Y doped samples was significantly noted. In general, Y doped samples showed most prominent weight change than La doped samples and pure sample. La doped samples exhibited lowest weight change among all. The decreases in Néel temperature with Y doping have been already reported (A. Gautam *et al*, 2012; X. K. Chen *et al*, 2012).

*XRD analyses*

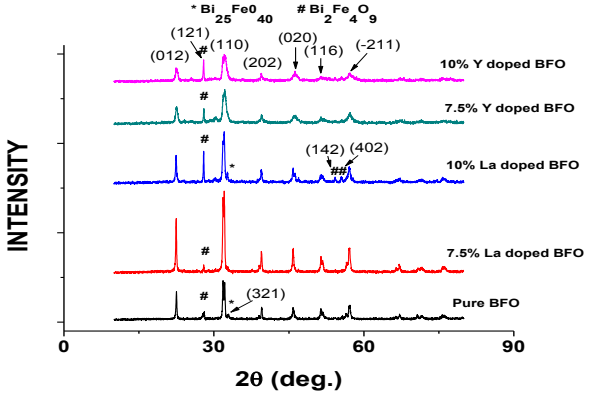


Figure 2: XRD curves of the prepared nanocrystallites of pure and doped BFO

Figure 2 shows the XRD result for the synthesized multiferroic materials. In reference to JCPDS No. 861518, 742493, 721832, 460416, it was found that the major peaks can be indexed to rhombohedral BFO and some minor peaks indicates the presence of impurity phases, namely, $Bi_{25}FeO_{40}$ and $Bi_2Fe_4O_9$. The presence of impurity was in accordance with the previous studies (Z. Chen *et al*, 2011; R. K. Mishra *et al*, 2008; M. B. Bellakki *et al*, 2010). It can be seen that the presence of impurity in the 10% La doped sample was much higher than the other samples. However in 10% Y doped sample, the impurity presence was comparatively lower than that of the 10% La doped sample. We can interpret that 10% is the solid solubility limit for the doped BFO (M. B. Bellakki *et al*, 2010). The particle sizes of the synthesized crystallites have been calculated using Scherrer's formula. It was found that for pure BFO, the crystallite size was 38.95nm and that for 7.5% Y doped BFO, it was 29.3nm. However, the particle size of the 10% Y doped sample was around 87nm. As the size of $Y^{3+}$ ion is less than that of the $Bi^{3+}$ ion and doping creates a substitutional solid solution where, the yttrium/lanthanum occupies bismuth site, so it was expected that the size of the Y doped samples would be less than that of the pure sample. However, increase in size with the 10% Y doped BFO can be attributed to the presence of significant amount of impurity in the sample. On the contrary, the size of $La^{3+}$ ion is greater than that of the $Bi^{3+}$ ion, so it was accordingly expected that the size of the La doped samples would be greater than that of the pure sample. The results confirmed the same, where we found that the size of the 7.5% La doped sample was 50.07nm and that of the 10% La doped sample was 50nm.

*Morphological analyses*

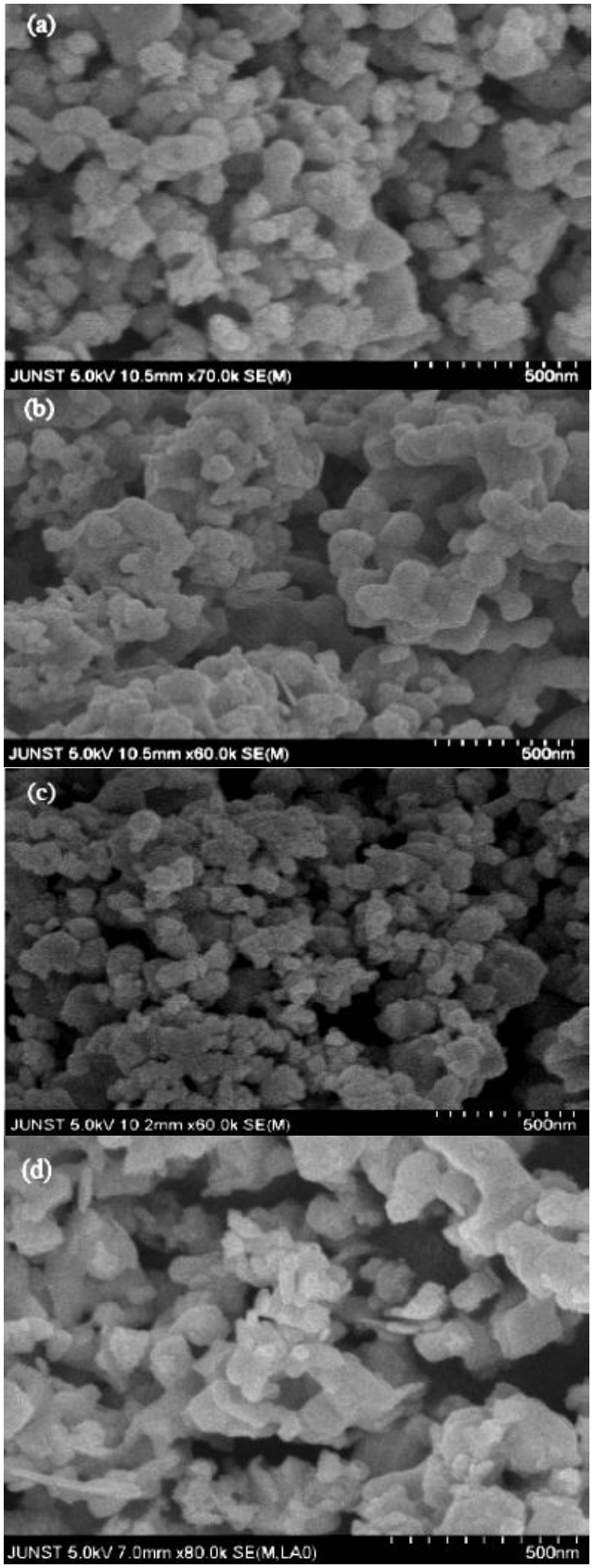

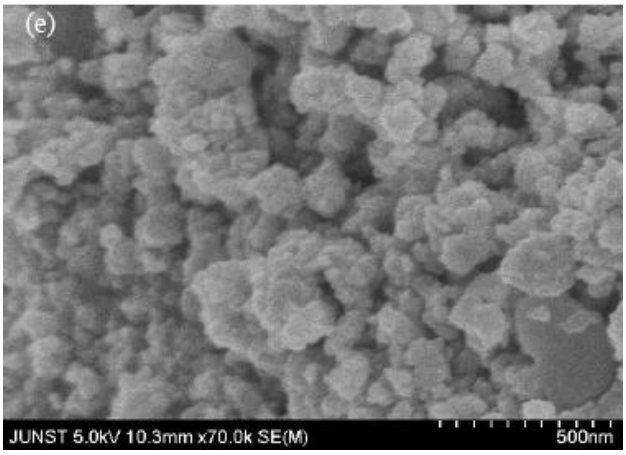


Figure 3: FESEM micrographs of a) pure BFO; b) 7.5% La doped BFO; c) 10% La doped BFO; d) 7.5% Y doped BFO; e) 10% Y doped BFO

Figure 3 shows the FESEM micrographs of the prepared crystallite samples. All of the samples showed agglomerated spherical kind of morphology which was in accordance with the previous studies (M. B. Bellakki *et al*, 2010; A. Gautam *et al*, 2012). The average particle sizes as calculated from the micrographs were in accordance to that calculated using Scherrer's formula. The average particle sizes for pure BFO, 7.5% La doped BFO, 10% La doped BFO, 7.5% Y doped BFO and 10% Y doped BFO were around 40.34nm, 51.43nm, 52.09nm, 30nm and 88.68nm respectively.

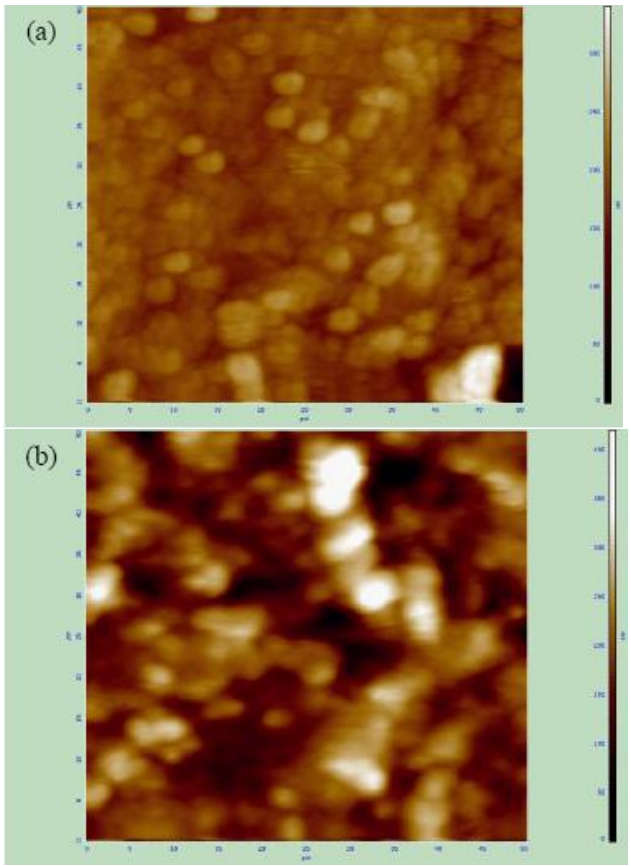


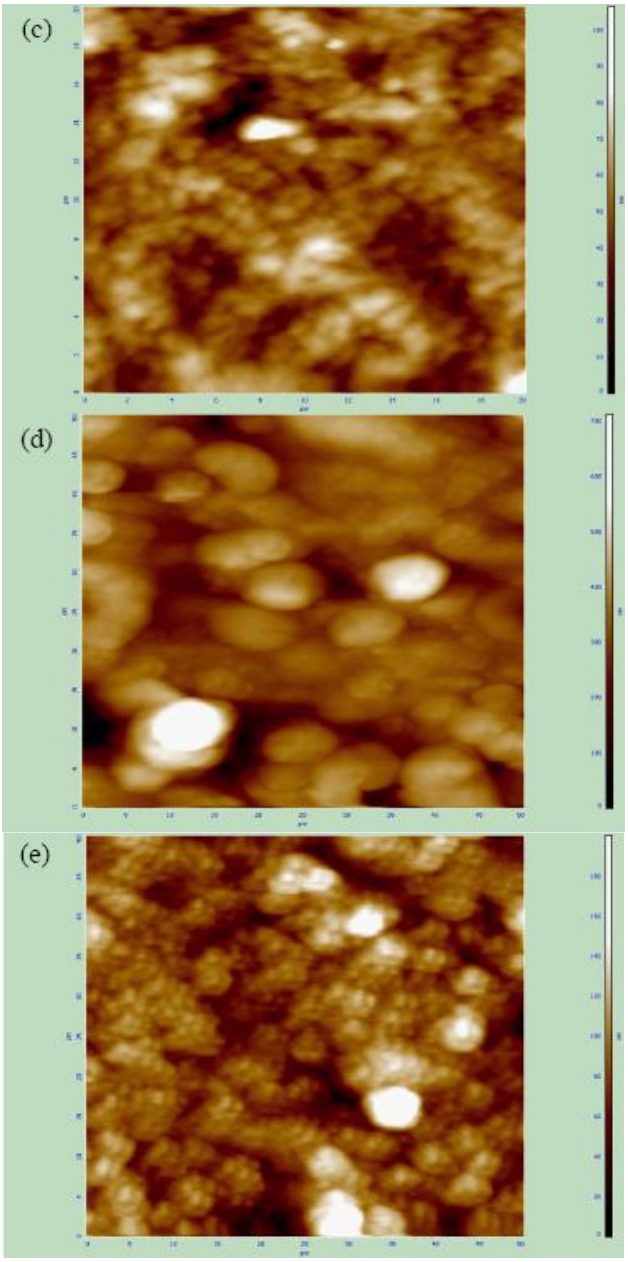


Figure 4: Two dimensional AFM micrographs of a) pure BFO; b) 7.5% La doped BFO; c) 10% La doped BFO; d) 7.5% Y doped BFO; e) 10% Y doped BFO

Figure 4 shows the two dimensional AFM images of the prepared samples. It can be seen that the samples show highly agglomerated spherical morphology with average particle size around the calculated values. The average roughness of the spin coated samples on the glass slides for pure BFO was 251nm and that of the 7.5% and 10% La doped nanocrystalline BFO was 91nm and 97nm respectively. On the other hand, the average roughness of 7.5% and 10% Y doped sample was 177nm and 195nm. Thus, it was evident that on doping the surface roughness gets improved. Roughness increases with doping concentration. La doped samples improved surface roughness than Y doped BFO. The three dimensional AFM images of the prepared samples have been shown in

figure 5. These images confirm the preferential agglomerated growth of the prepared crystallites.

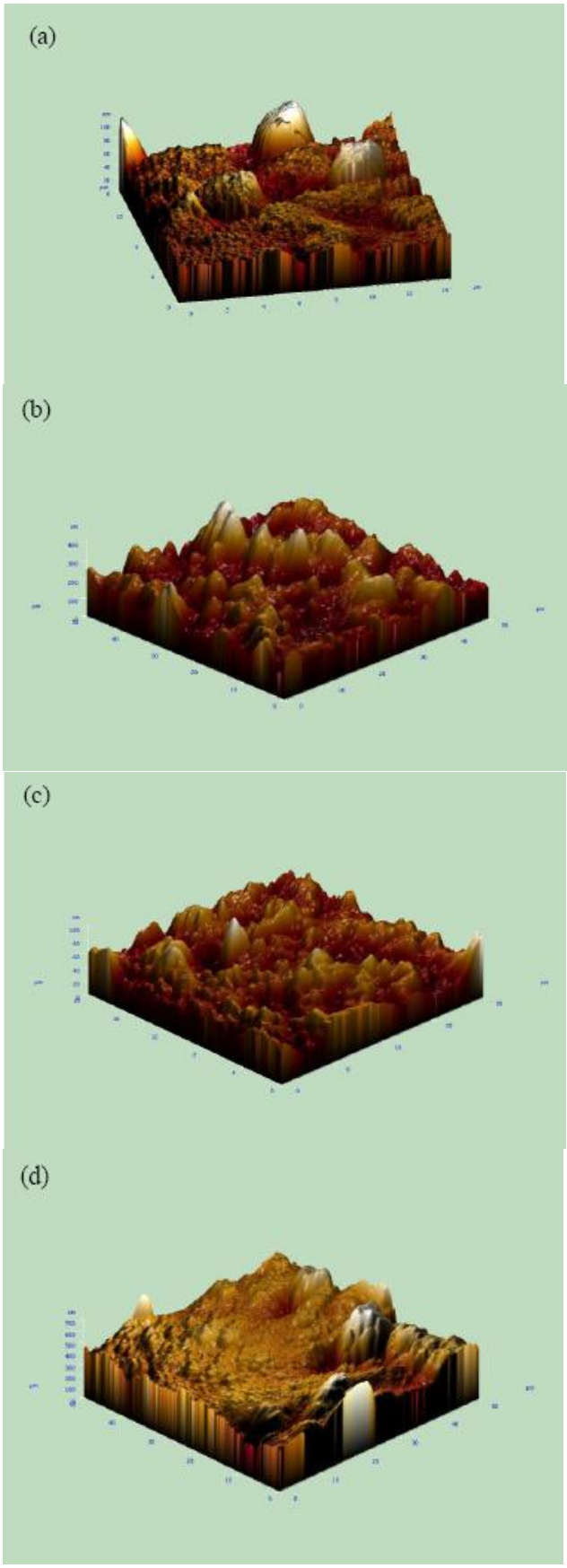


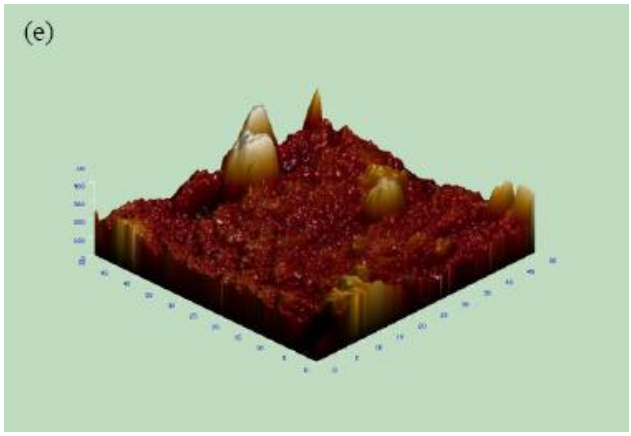


Figure 5: Three dimensional AFM micrographs of a) pure BFO; b) 7.5% La doped BFO; c) 10% La doped BFO; d) 7.5% Y doped BFO; e) 10% Y doped BFO

*UV-VIS analyses*

Figure 6 shows the UV-Vis spectra of the pure and the doped samples. The analyses of the curves show that the electronic band structure of BFO can be tuned. The band gap of pure nanocrystalline BFO was found to be 3.10ev while that of 7.5% Y doped BFO was 3.74ev and 10% Y doped BFO exhibited a band gap of around 3.9ev. This kind of progressive increase of band gap with Y doping has been observed by A. Mukherjee *et al*, 2012. In contrast, doping with La resulted in a decrease of band gap compare to pure BFO. The band gap of 7.5% La doped sample and 10% La doped sample were respectively 3.04ev and 2.4ev. The decrease in band gap due to rare earth transition metal doping has also been reported (M. B. Bellakki *et al*, 2010). A secondary peak around 450nm was seen in the samples. This could be due to metal to metal or ligand to metal charge transfers (A. Mukherjee *et al*, 2012). For further insights into the cause of these secondary effects, XPS studies need to be done to verify the electronic state of iron. This observation shows that doped bismuth ferrite samples have enhanced photo catalytic activity. In a study, the photo catalytic decomposition of organic contaminant Rhodamine-B by Y doped BFO has been successfully demonstrated (A. Mukherjee *et al*, 2012).

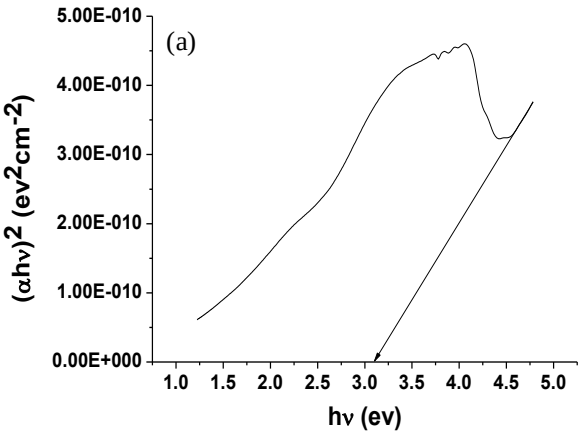

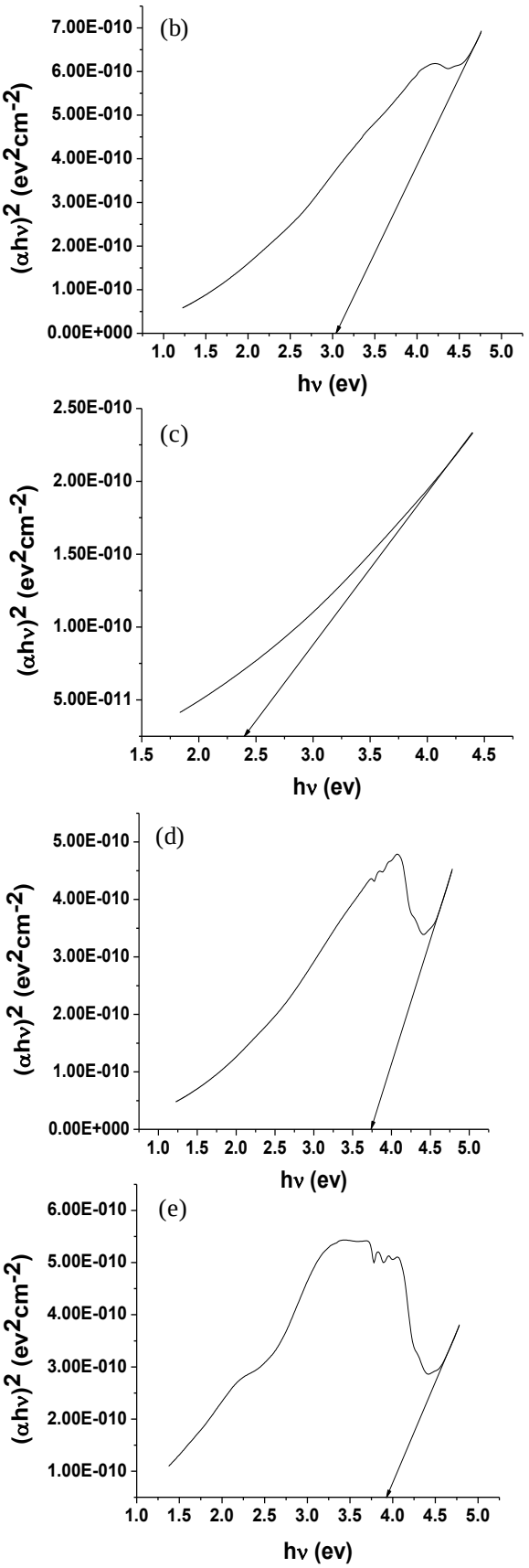


Figure 6: UV-VIS spectra of a) pure BFO; b) 7.5% La doped BFO; c) 10% La doped BFO; d) 7.5% Y doped BFO; e) 10% Y doped BFO

## Conclusion

The pure and doped BFO samples were synthesized successfully through chemical solution route. XRD studies showed rhombohedral structure with R3c space group with a spherical agglomerated morphology from FESEM. The ultrasonicated solution of the samples, spin coated on glass slides showed an improvement in surface roughness on doping. La doping exhibits the most improved roughness among all. UV-VIS analyses of the samples showed that the electronic band gap of BFO can be tuned and thus, the material holds great promise for photo catalytic activities in visible range. For studying the efficacy of BFO in sensor or memory applications, the multiferroic properties of the sample need to be studied.

## Acknowledgements

We are indebted to Dr. K. K. Chattopadhyay, Thin Film and Nanoscience Laboratory, Jadavpur University and his team of scholars for helping us in carrying out FESEM studies. We would also like to express our gratitude towards Metallurgical and Material Engineering Department, Jadavpur University for providing us with the characterization facilities. One of the authors would also like to thank DST-Nanomission, GOI for providing financial support.

## References

G. Catalan and J. F. Scott (2009), Physics and Applications of Bismuth Ferrite, *Advanced Materials*, Vol. 21, pp. 2463-2485.

Y. Yao, W. Liu, Y. Chan, C. Leung, C. Mak, and B. Ploss (2011), Studies of Rare-Earth-Doped $BiFeO_3$ Ceramics, *International Journal of Applied Ceramic Technology*, Vol. 8, No. 5, pp. 1246–1253.

F. Gao, C. Cai, Y. Wang, S. Dong, X. Y. Qiu, G. L. Yuan, Z. G. Liu, and J. –M. Liu (2006), Preparation of La-Doped $BiFeO_3$ Thin Films with $Fe^{2+}$ Ions on Si Substrates, *Journal of Applied Physics*, Vol. 99, pp. 094105-1–094105-4.

S. R. Das, P. Bhattacharya, R. N. P. Choudhary, and R. S. Katiyar (2006), Effect of La Substitution on Structural and Electrical Properties of $BiFeO_3$ Thin Film, *Journal of Applied Physics*, Vol. 99, pp. 066107-1–066107-3.

F. Yan, T. J. Zhu, M. O. Lai, and L. Lu (2010), Enhanced Multiferroic Properties and Domain Structure of La-Doped $BiFeO_3$ Thin Films, *Scripta Materialia*, Vol. 63, pp. 780–783.

M. Hojamberdiev, Y. Xu, F. Wang, W. Liu, and J. Wang (2009). La-Modification of Multiferroic $BiFeO_3$ by Hydrothermal Method at Low Temperature, *Inorganic Materials*, Vol. 45, No. 10, pp. 1183–1187.

Z. Chen, J. Hu, Z. Lu, and X. He (2011), Low-Temperature Preparation of Lanthanum-Doped $BiFeO_3$ Crystallites by a Sol–Gel–Hydrothermal Method, *Ceramics International*, Vol. 37, pp. 2359–2364.

A. Chaudhuri, and K. Mandal (2012), Enhancement of Ferromagnetic and Dielectric Properties of Lanthanum Doped Bismuth Ferrite Nanostructures, *Materials Research Bulletin*, Vol. 47, pp. 1057–1061.

X. Yan, J. Chen, Y. Qi, J. Cheng, and Z. Meng (2010), Hydrothermal Synthesis and Characterization of Multiferroic $Bi_{1-x}La_xFeO_3$ Crystallites, *Journal of the European Ceramic Society*, Vol. 30, pp. 265–269

Y. Du, Z. X. Cheng, M. Shahbazi, E. W. Collings, S. X. Dou, and X. L. Wang (2010), Enhancement of Ferromagnetic and Dielectric Properties in Lanthanum Doped $BiFeO_3$ by Hydrothermal Synthesis, *Journal of Alloys and Compounds*, Vol. 490, pp. 637–641.

M. B. Bellakki, and V. Manivannan (2010), Citrate-Gel Synthesis and Characterization of Yttrium-Doped Multiferroic $BiFeO_3$, *Journal of Sol–Gel Science and Technology*, Vol. 53, pp. 184–192.

A. Gautam, P. Uniyal, K. L. Yadav, and V. S. Rangra (2012), Dielectric and Magnetic Properties of $Bi_{1-x}Y_xFeO_3$ Ceramics, *Journal of Physics and Chemistry of Solids*, Vol. 73, pp. 188–192.

X. K. Chen, Y. J. Wu, J. Zhang, and X. J. Chen (2012), Giant Magnetic Enhancement across a Ferroelectric–Antiferroelectric Phase Boundary in $Bi_{1-x}Y_xFeO_3$, *Science China–Physics, Mechanics, & Astronomy*, Vol. 55, No. 3, pp. 404–408.

R. K. Mishra, D. K. Pradhan, R. N. P. Choudhary, and A. Banerjee (2008), Effect of Yttrium on Improvement of Dielectric Properties and Magnetic Switching Behavior in $BiFeO_3$, *Journal of Physics: Condensed Matter*, Vol. 20, pp. 045218-1–045218-6.

A. Mukherjee, S. M. Hossain, M. Pal, and S. Basu (2012), Effect of Y-doping on Optical Properties of Multiferroics $BiFeO_3$ Nanoparticles, *Applied Nanoscience*, DOI 10.1007/s13204-012-0114-8.